MODEL COMPUTATIONS OF VERTICAL MOTION IN THE UPPER TROPOSPHERE AND LOWER STRATOSPHERE FROM WIND POTENTIAL DATA

JERRY DEAN JARRELL

MODEL COMPUTATIONS OF VERTICAL MOTION IN THE UPPER TROPOSPHERE AND LOWER STRATOSPHERE FROM WIND POTENTIAL DATA

by

Jerry Dean Jarrell
Lieutenant Commander, United States Navy
B.S., Concord College, 1956

Submitted in partial fulfillment of the
requirements for the degree of

MASTER OF SCIENCE IN METEOROLOGY

from the

NAVAL POSTGRADUATE SCHOOL
June 1967

ABSTRACT

Fields of the potential function which had been obtained previously by Martin (1964), by numerical solution of a Poisson type equation were employed in this paper to obtain the divergence of the wind field at each grid point. Based upon a vertical interpolating polynomial formula for divergence, vertical integration of the divergence fields is performed from the top of the atmosphere to determine values of vertical motion at each grid point on the 50, 100, 200 and 300 mb levels. Features of these fields are discussed.

TABLE OF CONTENTS

LIST OF TABLES

LIST OF ILLUSTRATIONS

LIST OF SYMBOLS

T	Temperature
p	Pressure
z	Countour height at a pressure surface
η	Absolute vorticity
ζ	Relative vorticity
f	Corolis parameter
f_1	Corolis parameter at 45^{o} North latitude
ω	Vertical motion in (x,y,p,t) coordinates
$\mathbf{V}$	Horizontal vector wind
$\nabla \cdot \mathbf{V}$	Horizontal velocity divergence at constant pressure
ρ	density
t	time
$\mathbf{V}_\psi$	Non-divergent vector wind
$\mathbf{V}_\chi$	Irrotational vector wind
χ	Velocity potential function
ψ	Stream function
∇	Horizontal gradient, del operator
∇^2	Laplacian operator
$J(A,B)$	Jacobian operator
$\hat{i}$	Horizontal unit vector in the x-direction
$\hat{j}$	Horizontal unit vector in the y-direction
$\hat{k}$	Vertical unit vector
g	Acceleration due to gravity
R_d	Gas constant for dry air (.287 Joules g^{-1} o_K-1)

d	Mesh length (381 km at $60^{\circ}N$)
m	Map factor $(1 + \sin 60^{\circ})/(1 + \sin \phi)$
ϕ	Latitude
i	grid column number
j	grid row number
Φ	Geopotential ($\Phi = gz$)
$\mathcal{J}$	Finite difference Jacobian operator without grid distance divisor
∇^2	Finite difference Laplacian operator without grid distance divisor
$[A_{i,j}]$	Nine point square matrix of values at grid points surrounding point $A_{i,j}$ in a field of values of A

$$[A_{i,j}] = \begin{bmatrix} A_{i-1,j+1} & A_{i,j+1} & A_{i+1,j+1} \\ A_{i-1,j} & A_{i,j} & A_{i+1,j} \\ A_{i-1,j-1} & A_{i,j-1} & A_{i+1,j-1} \end{bmatrix}$$

1. Introduction

A number of diagnostic methods for computation of large-scale vertical motions are used operationally for feedback into prognostic models, for example, in the Cressman 3-level baroclinic model (2), and the Schuman 3-level primitive equation model (10). In both the diagonstic and prognostic approaches, Lorenz (3) has emphasized that certain energetic constraints must be invoked, one of which is the use of the "balance equation" for the determination of the purely rotational part of the wind. Lorenz also gives energetically consistent forms of the vorticity and thermodynamic equations, along with the appropriate version of the balance equation. Martin (4) has applied the Lorenz modeling system (omitting the thermodynamic equation) to determine the divergent part of the wind field from the 12-hour averaged vorticity equations. This resulted in the solution of the so-called CHI-2 equation to give 12-hour average values of the velocity potential over the octagonal 1977-point NMC grid, at each of three levels, 100, 200 and 300 mb.

The process was originally restricted by Martin to these upper levels in order to study the nature of the "spring" mass and temperature reversals in the stratosphere and the coupling of these effects with events in the upper troposphere. For that time (April 1963), hydrostatically consistent NMC data were not available above 100 mb so that two vertical modeling assumptions linking the fields of divergence at the various levels have been made in preference to the top-information-level approximation with subscript "1" denoting 100 mb.

$$\omega_1 \doteq -\tfrac{1}{2} P_1 \nabla \cdot V_1$$

Fields of divergence, and of the resulting vertical motions, time-centered at 0600 and 1800GMT for each of 1, 2, and 3 April 1963 have been deduced, and considered from the standpoints of vertical consistency as well as that of time-continuity. The meridional profile of the time-averaged zonal divergence and vertical velocities for the first six days in the same month is computed, and a theoretical mechanism for the mass-redistribution characteristics of stratospheric winter-to-summer reversal is set forth.

2. Computational Operations

The computations herein described were made on the CDC 1604 computer. The fields are on the NMC 1977-point octagonal grid. Two boundaries were recognized, the outer array of grid points where the wind potential and divergence were constrained to be identically zero. The particular forms of the del-square and Jacobian operators employed here are exactly as used in the preliminary solution procedure of the balance equation, (after Schuman (9)) which led to the χ -fields. This procedure is based upon the use of a nine-point module over the entire field, except on the computational boundary, where it is not possible to form the Schuman-version of the del-square operator. On the computational boundary, the values of ∇^2 and of $\mathcal{J}$ used here, as well as in Martin's solution (4)of the balance equation, was based upon a five-point module.

3. Velocity Potential

Stream function (ψ) fields were derived by numerical solution, in terms of geopotential ($\Phi = gz$), of the balance equation:

$$\nabla \cdot (f \nabla \psi) + 2(\psi_{xx}\psi_{yy} - \psi_{xy}^2) = \nabla^2 \Phi \qquad (1)$$

subject to appropriate convergence of the numerical solution at all grid points. The boundary condition was:

$$\frac{1}{f}\frac{\partial \psi}{\partial s} = \frac{1}{f}\frac{\partial \Phi}{\partial s}$$

where s is the arc length on the boundary.

Martin computed wind velocity potential (χ) fields by interative solution to the following Poisson type equation:

$$\tilde{\tilde{\eta}}\,\nabla^2 \tilde{\tilde{\chi}}^{(n)} = \left\{ -\left[\tilde{\tilde{\nabla^2 \frac{\partial \psi}{\partial t}}} + \tilde{\tilde{J(\psi, \eta)}} \right] - \tilde{\tilde{\nabla \eta}} \cdot \nabla \tilde{\tilde{\chi}}^{(n-1)} \right\} \qquad (2)$$

where the superscript n refers to the iteration number. The symbol ($\tilde{\tilde{\ }}$) denotes a 12-hour time mean quantity. The terms enclosed within the bracket on the right side constitute the full forcing function for the first interation $\tilde{\tilde{\chi}}^{(1)}$, after which Liebmann sequential relaxation yielded the final convergent fields within a maximum of nine iterations. The solution of (2) gave 12-hour mean χ-fields for 0600 and 1800GMT at the 100, 200, and 300 mb levels for April 1-6, 1963.

4. Horizontal divergence in (x,y,p,t) coordinates.

Since $\mathbf{V} = \hat{k} \times \nabla\psi + \nabla\chi$ is a valid expression for the horizontal wind, it follows that

$$\nabla \cdot \mathbf{V} = \nabla \cdot \nabla\chi = \nabla^2 \chi$$

Since χ has dimensions L^2T^{-1}, it is convenient to multiply by f_1/g thus forming the scaled quantity $\hat{\chi}$ in units of cm. Thus printouts of the $\hat{\chi}$-fields are of the same dimensions as countour heights. Then in finite difference notation, $\nabla^2\chi$ becomes:

$$\nabla^2\chi = gm^2(f_1 d^2)^{-1} \nabla^2\hat{\chi}$$

$\nabla^2\chi$ is defined as follows, in conformity with the operator used previously in the balance equation solution.

A. On the outer boundary

$$\nabla^2\chi_{ij} \equiv 0$$

B. On the computational boundary

$$\nabla^2\chi_{ij} = \frac{1}{2}\begin{bmatrix} 0 & 1 & 0 \\ 1 & -4 & 1 \\ 0 & 1 & 0 \end{bmatrix}\left[\chi_{ij}\right]$$

C. For interior points

$$\nabla^2\chi_{ij} = \frac{1}{2}\begin{bmatrix} 1 & 0 & 1 \\ 0 & -4 & 0 \\ 1 & 0 & 1 \end{bmatrix}\left[\chi_{ij}\right]$$

At most, two of the points used in the operator defined in B above, are non-zero, and the central point will always be zero resulting in unrealistically large values of $\nabla^2\chi$. The factor 1/2 was used to provide a slower trend toward the inherently larger $\nabla^2\chi$ values on the computational boundary.

Only the divergence fields were smoothed. Smoothing was accomplished by making two separate passes over all $\nabla^2\chi$ using,

on each pass, a smoothing operator ($\overline{}$) defined as follows:

A. For points on the outer boundary the smoothed values were constrained to be identically zero.

B. For points on the computational boundary

$$(\overline{\nabla^2\chi})_{ij} = \frac{1}{8}\begin{bmatrix} 0 & 1 & 0 \\ 1 & 4 & 1 \\ 0 & 1 & 0 \end{bmatrix}\left[\nabla^2\chi_{ij}\right]$$

C. For interior points

$$(\overline{\nabla^2\chi})_{ij} = \frac{1}{16}\begin{bmatrix} 1 & 2 & 1 \\ 2 & 4 & 2 \\ 1 & 2 & 1 \end{bmatrix}\left[\nabla^2\chi_{ij}\right]$$

5. Vertical Motion in (x,y,p,t) coordinates.

Extensive use is made of the continuity equation,

$$-\frac{\partial\omega}{\partial p} = \nabla^2\chi \tag{3}$$

which may be integrated from the top of the atmosphere (p=0) to some arbitrary pressure level p.

$$\omega(p) - \omega(0) = -\int_0^p \nabla^2\chi\,\delta p = \int_0^p \frac{\partial\omega}{\partial p}\,\delta p \tag{4}$$

The following pair of upper boundary conditions are assumed: both ω and $\nabla^2\chi$ are zero at p = 0. Then equation 4 reduces to

$$\omega(p) = \int_0^p \frac{\partial\omega}{\partial p}\,\delta p \tag{5}$$

To define a reasonable function of pressure

$$\frac{\partial\omega}{\partial p} = f(p) \tag{6}$$

one can pass an interpolating polynomial in p through the known values of $\frac{\partial \omega}{\partial p}$ at each vertical grid point, and then integrate this polynomial. However, in order to give an additional condition in the vertical, we have already assumed that $\frac{\partial \omega}{\partial p} = 0$ at $p = 0$. The implications of this are reasonable and will be discussed later.

A Lagrangian interpolating polynomial was chosen in the form

$$L(p) = \sum_{i=0}^{n} \frac{\Pi_{(i)}(p)}{\Pi_{(i)}(p_i)} f(p_i) \tag{7}$$

where $\Pi_{(i)}(p) = (p-p_0)(p-p_1)\cdots(p-p_{i-1})(p-p_{i+1})\cdots(p-p_n)$

and the $f(p_i)$ are the known values of $\frac{\partial \omega}{\partial p}$ at the level where $p = p_i$. Then using the notation $\omega_{p_n} = \frac{\partial \omega}{\partial p}$ at level n, where n = 0,1,2,3 corresponding to pressure levels p = 0 , 100, 200, and 300 mb, (and $p = p_n$ at level n), leads to

$$\frac{\partial \omega}{\partial p} = \frac{(p-p_1)(p-p_2)(p-p_3)}{(p_0-p_1)(p_0-p_2)(p_0-p_3)}\omega_{p_0} + \frac{(p-p_0)(p-p_2)(p-p_3)}{(p_1-p_0)(p_1-p_2)(p_1-p_3)}\omega_{p_1}$$

$$+ \frac{(p-p_0)(p-p_1)(p-p_3)}{(p_2-p_0)(p_2-p_1)(p_2-p_3)}\omega_{p_2} + \frac{(p-p_0)(p-p_1)(p-p_2)}{(p_3-p_0)(p_3-p_1)(p_3-p_2)}\omega_{p_3} \tag{8}$$

by the upper boundary condition, $\omega_{p_0} = 0$. Also $p_2 = 2p_1$ and $p_3 = 3p_1$ for substitution into eq 8 and one obtains:

$$\omega_p = \frac{p^3 - 5p_1p^2 + 6p_1^2p}{2p_1^3}\omega_{p_1} - \frac{p^3 - 4p_1p^2 + 3p_1^2p}{2p_1^3}\omega_{p_2} + \frac{p^3 - 3p_1p^2 + 2p_1^2p}{6p_1^3}\omega_{p_3} \tag{9}$$

Upon integrating eq 9 from p = 0 to p = p, and factoring $(1/2)p_1$, results in ω_p as a function of pressure.

$$\omega(p) = \tfrac{1}{2}p_1\left\{\left[\tfrac{1}{4}\left(\tfrac{p}{p_1}\right)^4 - \tfrac{5}{3}\left(\tfrac{p}{p_1}\right)^3 + 3\left(\tfrac{p}{p_1}\right)^2\right]\omega_{p_1}\right.$$
$$- \left[\tfrac{1}{4}\left(\tfrac{p}{p_1}\right)^4 - \tfrac{4}{3}\left(\tfrac{p}{p_1}\right)^3 + \tfrac{3}{2}\left(\tfrac{p}{p_1}\right)^2\right]\omega_{p_2} \qquad (10)$$
$$\left. + \left[\tfrac{1}{12}\left(\tfrac{p}{p_1}\right)^4 - \tfrac{1}{3}\left(\tfrac{p}{p_1}\right)^3 + \tfrac{1}{3}\left(\tfrac{p}{p_1}\right)^2\right]\omega_{p_3}\right\}$$

Now $-\omega_{p_n} = \nabla^2\chi_n$ where $\nabla^2\chi_n$ is the twice-smoothed finite-difference expression for divergence at level p_n. When p in eq. 10 is successively set equal to 50, 100, 200 and 300 mb, and replacing $(1/2)p_1$ by 50 mb, the following set of equations, in matrix notation, results

$$\begin{bmatrix}\omega_{.5}\\ \omega_1\\ \omega_2\\ \omega_3\end{bmatrix} = -(50)\begin{bmatrix}\frac{107}{192} & -\frac{43}{192} & \frac{9}{192}\\ \frac{19}{12} & -\frac{5}{12} & \frac{1}{12}\\ \frac{8}{3} & \frac{2}{3} & 0\\ \frac{9}{4} & \frac{9}{4} & \frac{3}{4}\end{bmatrix}\begin{bmatrix}\nabla^2\chi_1\\ \nabla^2\chi_2\\ \nabla^2\chi_3\end{bmatrix} \qquad (11)$$

in units of mb(sec)$^{-1}$.

6. Some Results of the Computations

The omega-vertical velocity fields.

Since $-\frac{\partial\omega}{\partial p} = \nabla\cdot\mathbf{V} = \nabla^2\chi$ is divergence in units of sec^{-1}, it is evident that eq 10 would normally lead to results in mb(sec)$^{-1}$; however, upon multiplying by 43,200, comparable results are in mb(12 hrs)$^{-1}$. It is desirable to be able to interpret omega-values in terms of geometric vertical velocity expressed by $w = \frac{dz}{dt}$, in units of cm(sec)$^{-1}$.

Expansion of ω in terms of x,y,z,t coordinates leads to

$$\frac{dp}{dt} = \frac{\partial p}{\partial t} + \nabla \cdot \nabla_H p + w \frac{\partial p}{\partial z} \doteq -g\rho (w - w_p) \qquad (12)$$

when the advective term is omitted. Here the notation $w_p = \left(\frac{\partial z}{\partial t}\right)_p$ has been employed, although this term is usually negligible compared to $\frac{dz}{dt}$. Hence w is related to ω through

$$w(\text{cm/sec}) = c - \frac{1}{\rho g}\omega \text{ (mb/12 hrs)}, \quad c = 1/43{,}200 \qquad (13)$$

By the equation of state, we have

$$\frac{1}{g\rho} = \frac{R_d T}{gp} = \frac{10^4 \text{cm}}{3.42^{\circ}\text{K}} \frac{T}{p} \qquad (14)$$

If it is assumed that temperature varies little in the vertical at levels from 300 to 50 mb, or $\frac{T}{T_m} = 1$, and that T_m equals 220°K*, then substituting 220°K for T in eq 14 gives the following approximation.

$$w(\text{cm/sec}) \doteq -\frac{15}{p}\omega \text{ (mb/12 hrs)}.$$

This result leads to the tabular conversion factors presented in Table 1.

p(mb)	w to ω 1 cm/sec	ω to w 10 mb/12 hrs
50	3.33 mb/12hrs	3.00 cm/sec
100	6.67 mb/12hrs	1.50 cm/sec
200	13.33 mb/12hrs	0.75 cm/sec
300	20.00 mb/12hrs	0.50 cm/sec

Table 1. Conversion factors mb/12hrs to cm/sec (magnitudes only)

*The actual temperature range is of the order of 200 to 235°K, and therefore is subject to a maximum error of 10%.

Centers of divergence (or convergence) of magnitudes on the order of $5 \times 10^{-5} sec^{-1}$ are evident around the boundary extending inward for six or so grid lengths, (see Figures 3, 4, and 5). Corresponding vertical motion centers also appear with magnitudes as high as 30 cm/sec, (see Figures 6 through 9 and Table 1). These centers may be partly due to contamination from the artificial boundary conditions employed in the forcing function side of the χ -2 equation. For example, due to boundary limitations, advection of vorticity was not possible on the outer, nor on the computational boundary thus accounting for $\chi = 0$ on both of these boundaries. It is doubtful that the atmosphere recognizes these limitations, and the effect of this assumption could have a tendency to increase the χ magnitudes and the resulting $\nabla^2 \chi$ computation magnitudes within the first few rows of points inward from the boundary.

Poleward of this boundary zone, magnitudes appear reasonable, having maximum central values corresponding to geometric velocities of around 10 cm/sec.

The values of ω either have a reduced magnitude at 50 mb, or exhibit a reversal in sign compared to those in the upper troposphere. This is a result induced by the assumptions $\omega = \frac{\partial \omega}{\partial p} = 0$ at $p = 0$. The upper condition $\frac{\partial \omega}{\partial p} = 0$ is reasonable at heights where, in general, synoptic-scale systems are likely to appear as "noise" superimposed upon a vigorous diurnal circulation (Craig (1)). More specifically during mid-April, the zonal and meridional wind components are slowing down, and then gradually reverse in sign on a very large

scale basis. As an example see the vertical profiles for Berlin (5) during April. If $u = 0$, $v = 0$ is applicable for the levels 30-40 km, then the approximation $\frac{\partial \omega}{\partial p} = 0$ appears to be particularly appropriate during a period encompassing the time of the stratospheric wind reversal.

Two spatial cross sections were taken on each of two map times (01/1800 and 02/0600GMT April 1963). The first was roughly west-to-east along grid points in a line connecting the positions 24.8N, 120.6W and 32.3N, 51.9W, beginning off Mexico in the Pacific, through Baja California, the southwestern United States and off the Virginia coast into the Atlantic to the east of Bermuda. This cross section consists of 22 grid points. Analyzed data, including divergence and omega at both times, is presented in Figure 11. The second cross section was taken south-to-north along 80^{o}W from a point off Miami (24.5^{o}N) to a point northwest of Thule, Greenland (78.4^{o}N). This data is similarly presented in Figure 12. These cross sections exhibited a vertical consistency in the divergence fields, and the resulting consistency, not unexpected by the model, in the omega fields. Despite the close relationship between the two sets of data, the slopes of centers and their relations are not obvious, and a real insight is gained by noting these slopes.

7. Time Continuity of the Vertical Motion Centers.

In studying time-continuity of the ω-fields, a test area encompassing North America and portions of the adjacent oceans was used. A time classification system based upon an alphabetical letter listing from A,...,L for $\omega > 0$ (downdraft) centers and M,...,Z for $\omega < 0$

(updraft) centers was employed. In addition a numerical code integer immediately following the letter identifies the particular chart number from 1,...,6 (0600 Apr. 1,...,1800GMT Apr. 3, 1963) upon which the specific lettered center was first identified within the test area. Note that a time-coding symbol such as A4 means that a particular ω-max center (positive) was first identified on map four (1800GMT Apr. 2). There was an earlier center A1, listed in Table 2, but there should be no ambiguity in examining Table 2 since this latter case was identified on map one, and its location and time-track for three successive periods is plainly noted. This system enables one to list all centers identified within the 26-alphabetic letters without ambiguity. Tracking of a particular center was continued only if it remained within the geographical test area, and was discontinued after the "exiting" map.

If two ω-centers merged into a single center, only the composite center was tracked thereafter, but for the purpose of counting, all merging centers were considered present until the combined center was lost either by its movement or dissipation.

In Table 2, there is listed a census of all positive centers identified and tracked, together with their locations by map time. A similar treatment for negative centers is presented in Table 3. Under "Time-Classification", there is also included, a "Remarks" column which lists reasons why tracking was discontinued and/or other pertinent information. The information applicable under "Remarks" is coded as a number 1,...,6 below.

1. Departed test area across indicated boundary (particular boundary in parenthesis).
2. Merged with indicated center, carried on subsequent maps as latter center (particular center in parenthesis).
3. Dissipated
4. Moved into boundary region south of 25°N.
5. Quasi-stationary
6. Was still present on final map.

Finally in both Tables 2 and 3, there is a column headed "Intensity Classification". This classification includes an alphabetic code for the maximum vertical motion at the level of greatest vertical motion.

(a) $|w| \geq 7.0$ cm-sec^{-1}

(b) $7 > |w| \geq 3.0$ cm-sec^{-1}

(c) $|w| < 3.0$ cm-sec^{-1}

There is also a following numeral (0,1,2,3,4) indicative of the number of levels at which closed omega-contours, at a contour interval of 1.5 cm-sec^{-1}, existed.

In addition to the census of omega-downdrafts and omega-updrafts which could be subjected to time-continuity (Tables 2 and 3), tabulations of the cumulative total of centers subject to possible tracking are shown in Table 4. Those subject to actual tracking are shown in Table 5, and percentages of those subject to possible tracking that tracked for one or more periods (Table 6). Note that between 0600 April 1 and 1800GMT April 3, there is a maximum of 60 tracking-hours, and that 37 of 42 centers could be tracked for at least one 12-hour period.

NO.	MAPS	TIME CLASSIFICATION Positions °N-°W 01/06Z	01/18Z	02/06Z	02/18Z	03/06Z	03/18Z	REMARKS	INTENSITY CLAS. IFICATION FIRST	LAST
A1	3	45-137	33-127	28-124				1(W),4	b3	
B1	1	23-104						1(S),4	b4	
C1	2	31-085	25-080					1(S),4	b3	b4
D1	2	49-059	46-052					2(E1)	c0	c0
E1	2	31-060	36-057					3	a2	b3
F1	6	48-104	43-089	39-076	44-068	48-065	56-059	6	c0	c0
G1	3	51-085	42-070	46-062				3	c0	b2
B2	4		46-140	45-131	30-124	24-112		1(S),4	c0	b3
H2	2		47-102	43-089				3	c0	c0
I2	3		36-077	28-064	33-053			3	b4	b3
J2	1		58-076					3	c0	
D3	1			26-094				2(H3)	b3	
E3	4			52-102	45-090	38-077	28-080	6	c0	a4
H3	4			29-081	32-081	28-082	28-082	5,6	b1	b4
K3	2			60-087	56-067			2(F1)	c0	c0
L3	1			43-099				2(E3)	c0	c0
A4	3				44-134	37-124	31-123	6	c0	c0
G4	1				34-098			2(H3)	b4	
H4	1				60-093			3	c0	
J4	2				61-027	61-026		5	c0	c0
G5	2					44-088	37-077	6	c0	c0
H5	1					32-059		1(E)	b4	
K5	2					49-140	49-142	6	b3	b1
L5	2					28-122	23-115	6	b3	c0

Table 2. Three day history of positive omega centers.

NO.	MAPS	TIME CLASSIFICATION Positions °N-°W 01/06Z	01/18Z	02/06Z	02/18Z	03/06Z	03/18Z	REMARKS	INTENSITY CLASSIFICATION FIRST	LAST
M1	2	30-097	24-096					1(S),4	b3	a4
N1	1	38-095						3	b2	
01	5	48-075	51-060	56-034	69-049	70-037		3	c1	c1
R1	4	31-111	36-099	35-089	36-079			3	b2	b2
S1	2	56-100	48-077					2(N2)	c0	c0
T1	2	64-046	69-073					3	c0	c0
U1	1	35-068						3	b1	
N2	4		55-105	52-093	46-079	35-067		1(E)	c0	a4
P2	2		26-068	25-055				1(SE),4	a4	b3
Q2	1		30-060					2(01)	c1	
V2	1		46-037					2(01)	c1	
W2	3		29-112	34-097	39-094			3	b2	b2
M3	4			48-144	36-148	42-149	43-151	6	b3	b2
P3	4			23-103	27-104	28-105	29-105	5,6	b2	b2
Q3	1			39-053				1(E)	b3	
S3	1			29-105				2(W2)	c0	
T3	2			48-075	37-062			1(E)	b1	b3
V3	1			35-068				1(SE)	b3	
X3	4			33-117	37-109	39-092	37-068	6	c0	a4
P4	3				56-124	55-127	55-129	5,6	c0	c0
Q4	2				43-103	45-068		3	b1	b1
S4	1				52-094			3	c1	

Table 3. Three day history of negative omega centers.

	60	48	36	24	12
Positive	3	6	12	17	22
Negative	5	9	14	17	20
Total	8	15	26	34	42

Table 4. Cumulative number of centers as a function of possible tracking time.

	60	48	36	24	12
Positive	1	1	7	12	20
Negative	0	2	9	11	17
Total	1	3	16	23	37

Table 5. Cumulative number of centers as a function of actual tracking time.

	60	48	36	24	12
Possitive	33.3	16.7	58.3	70.6	90.9
Negative	0.0	22.2	64.2	64.8	85.0
Total	12.5	20.0	61.6	67.8	88.1

Table 6. Cumulative per cent of possible centers actually tracked as a function of available tracking time.

In tracking positive or negative omega-centers in the geographical area under consideration, first preference was ascribed to a downwind direction, and second to choose a center that existed at the same number of levels (intensity classification) as on the previous map set. This sometimes meant looking crosswind, or at a stationary system. For an example of detailed tracking, one particular center (F1, Table 2) was present on all six map-sets. Table 7 presents its 12-hourly positions as well as central values at each of the four pressure levels considered in this study. The movement of this center closely paralleled the 300 mb wind from its first appearance as a weak center of descending motion at 300 mbs on April 1 at 0600GMT, over the Great Plains until it reached the coast near Washington, D. C. 24 hours later, as a strong subsidence center at all levels. During the next 36 hours it appeared to move cross-flow toward the northeast along the New England coast then along the Canadian coast staying well upstream of a deep 300 mb trough along 50^{o}W. Toward the end of this latter period it became disorganized.

In order to set the background conditions relating to the period of this study, the initial 300 and 100 mb contour analyses are provided in Figures 1 and 2 respectively for 0000GMT April 1, 1963, (8) and (7).

8. Zonal Means.

During the winter the stratospheric Northern hemisphere is a cold low pressure area with a strongly baroclinic vortex and basically westerly flow, whereas the summer is just the opposite with a warm polar high and easterly flow. Thus we expect, at some upper level, the

TIME	PRESSURE LEVEL 300 mb	200 mb	100 mb	50 mb
01/06Z	48.3N 104.0W	48.0N 104.0W	49.0N 104.0W	49.0N 104.0W
	+37mb/12hrs	*	*	*
01/18Z	43.1N 88.6W	44.0N 88.5W	49.0N 88.0W	44.7N 88.3W
	+86mb/12hrs	+41mb/12hrs	*	+ 2mb/12hrs
02/06Z	38.6N 75.5W	38.9N 75.0W	42.0N 70.0W	41.0N 69.0W
	+53mb/12hrs	+29mb/12hrs	*	*
02/18Z	43.9N 68.3W	43.2N 68.9W	42.9N 66.9W	42.0N 68.0W
	+100mb/12hrs	+58mb/12hrs	+18mb/12hrs	+ 5mb/12hrs
03/06Z	47.9N 65.4W	47.4N 67.7W	46.0N 67.0W	46.0N 66.0W
	+44mb/12hrs	+19mb/12hrs	*	*
03/18Z	56.1N 58.6W	52.0N 55.0W	51.1N 60.7W	51.0N 62.0W
	+19mb/12hrs	*	+13mb/12hrs	*

Table 7. Detailed 4-level history of a selected omega center. Positions given as a function of time and pressure level. (* indicates no closed contours were present at this time-level, position estimated from contour ridging.)

mid-winter stratosphere to be convergent and the mid-summer hemisphere divergent. The mean meridional circulation in April should be a transition between these opposing pictures. Meridional profiles of the divergence patterns and associated vertical motions are depicted in Figure 10. The values computed are based upon zonally averaged values taken throughout the region of this study, then averaged for the whole six day period. Resulting values are taken as valid from 20°N to the pole, and the profiles are intended to be suggestive of the mean meridional circulation during the stratospheric transition period.

Intense ozone heating in the upper stratosphere appears to be eliminating the polar low in most of the high latitudes, particularly at high levels. The intense tropospheric convergence at the pole is probably induced by "spillover" from the surrounding divergent areas, especially where the ozone-heating is so prominent (after Pressman (6)). The summer anticyclone is becoming established from aloft as evidenced by the convergence area above 200 mb near 85°N. The mid-latitude stratosphere is an area of rather weak divergence, indicative of the general "slow-down" associated with the "spring-reversal". The convergence in the northern edge of the tropics is probably due to the cross-equator flow from the divergent north, and also in support of the sub-tropical anticyclone below, which by (8) remained quasi-stationary for the entire period near 10°N at 300 mb.

Figure 1. 300 mb height analysis, 010000GMT April 1963

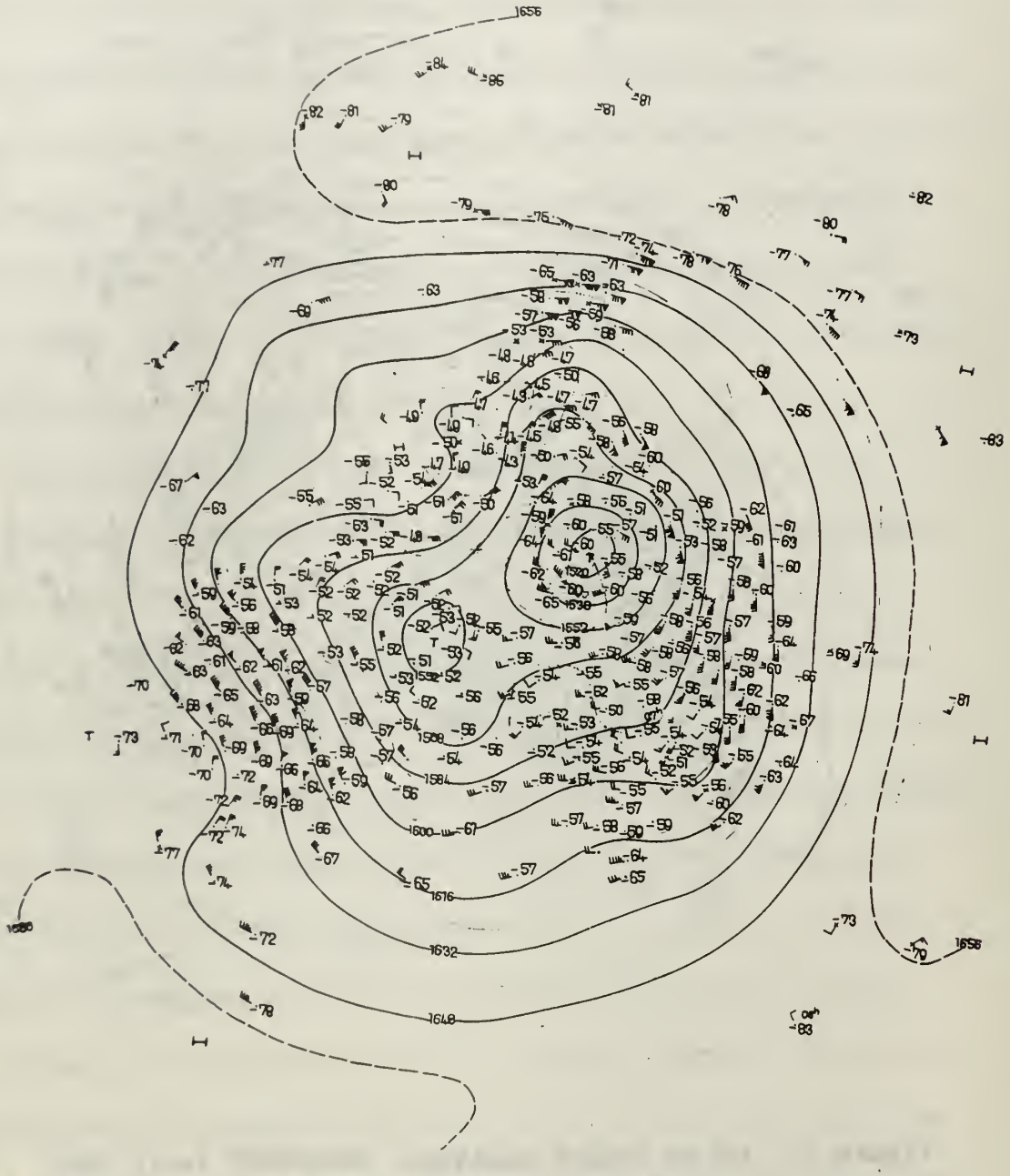

Figure 2. 100 mb height analysis, 010000GMT April 1963

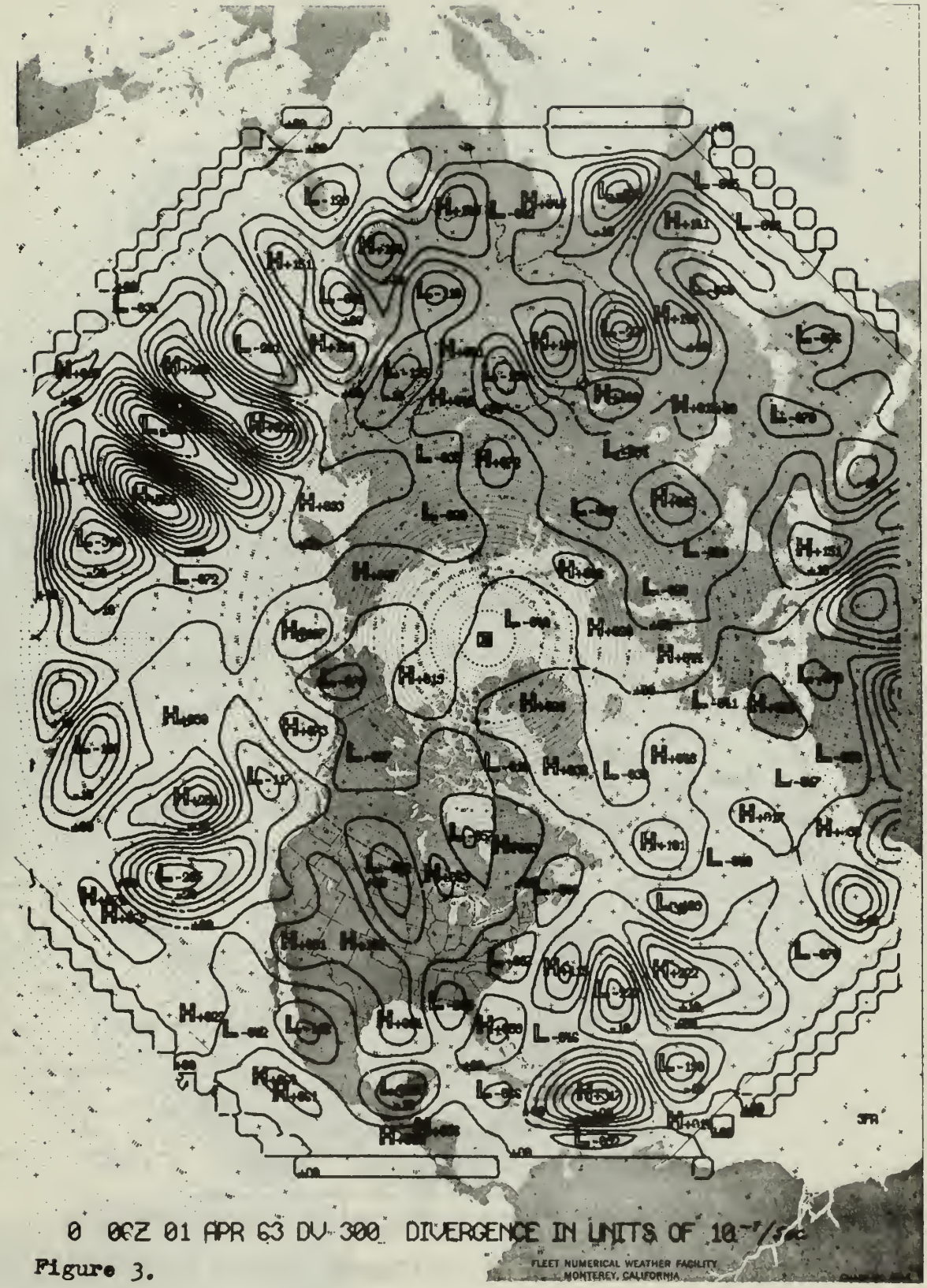
0 00Z 01 APR 63 DV 300 DIVERGENCE IN UNITS OF 10⁻⁷/sec
FLEET NUMERICAL WEATHER FACILITY
MONTEREY, CALIFORNIA

Figure 3.

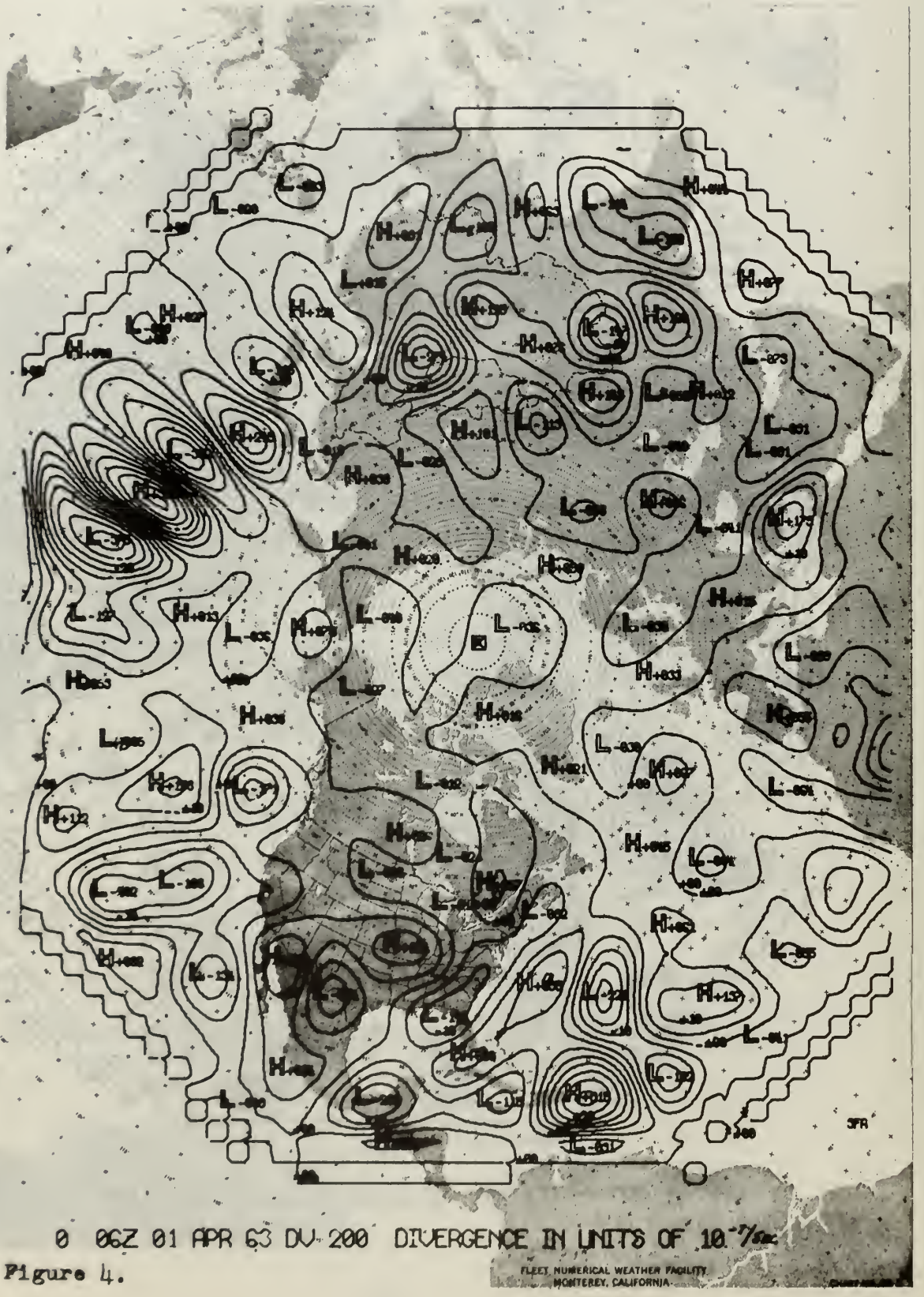
0 06Z 01 APR 63 DV 200 DIVERGENCE IN UNITS OF 10⁻⁷/sec
FLEET NUMERICAL WEATHER FACILITY
MONTEREY, CALIFORNIA

Figure 4.

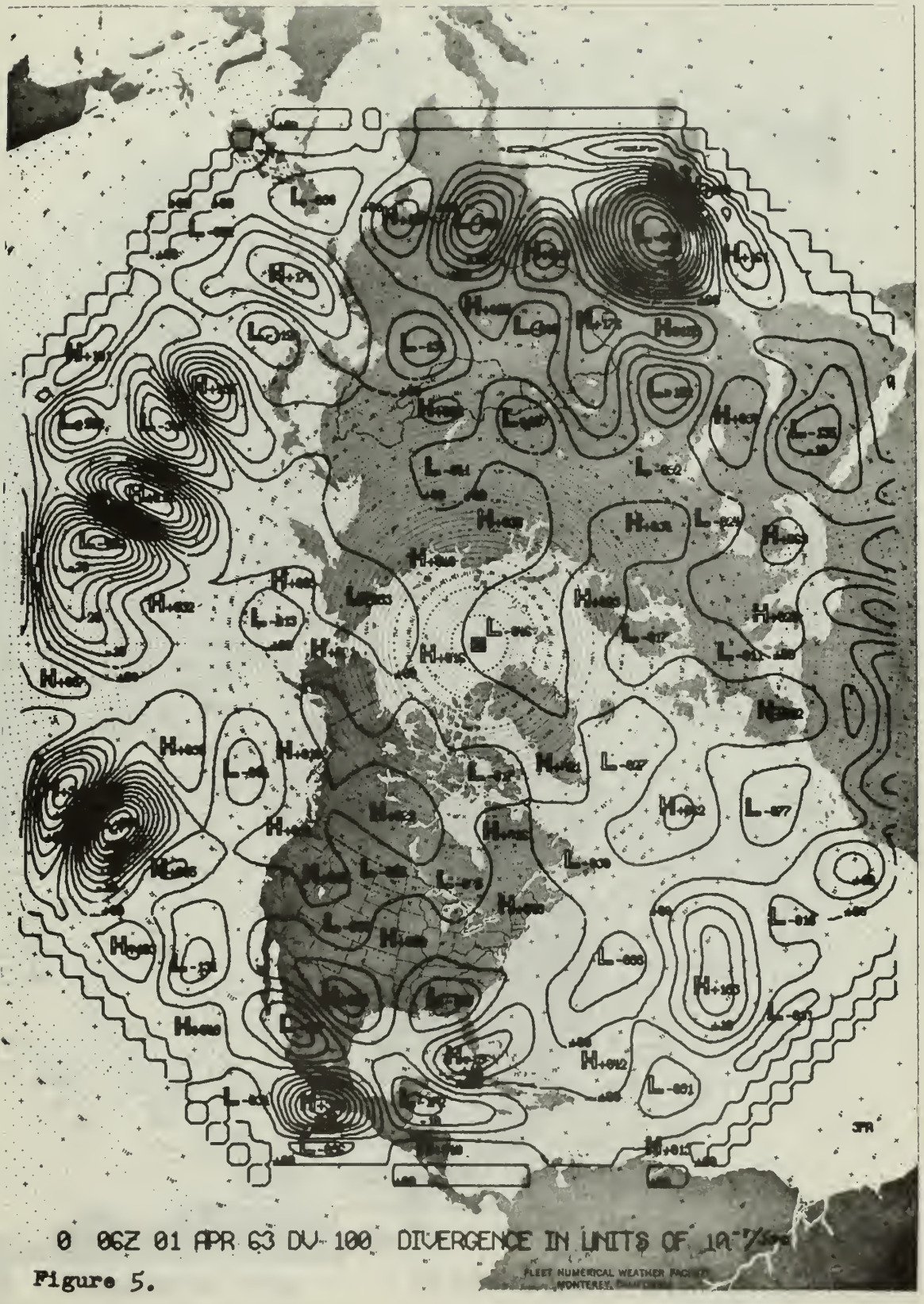
0 06Z 01 APR 63 DV 100 DIVERGENCE IN UNITS OF 10
FLEET NUMERICAL WEATHER FACILITY
MONTEREY, CALIFORNIA

Figure 5.

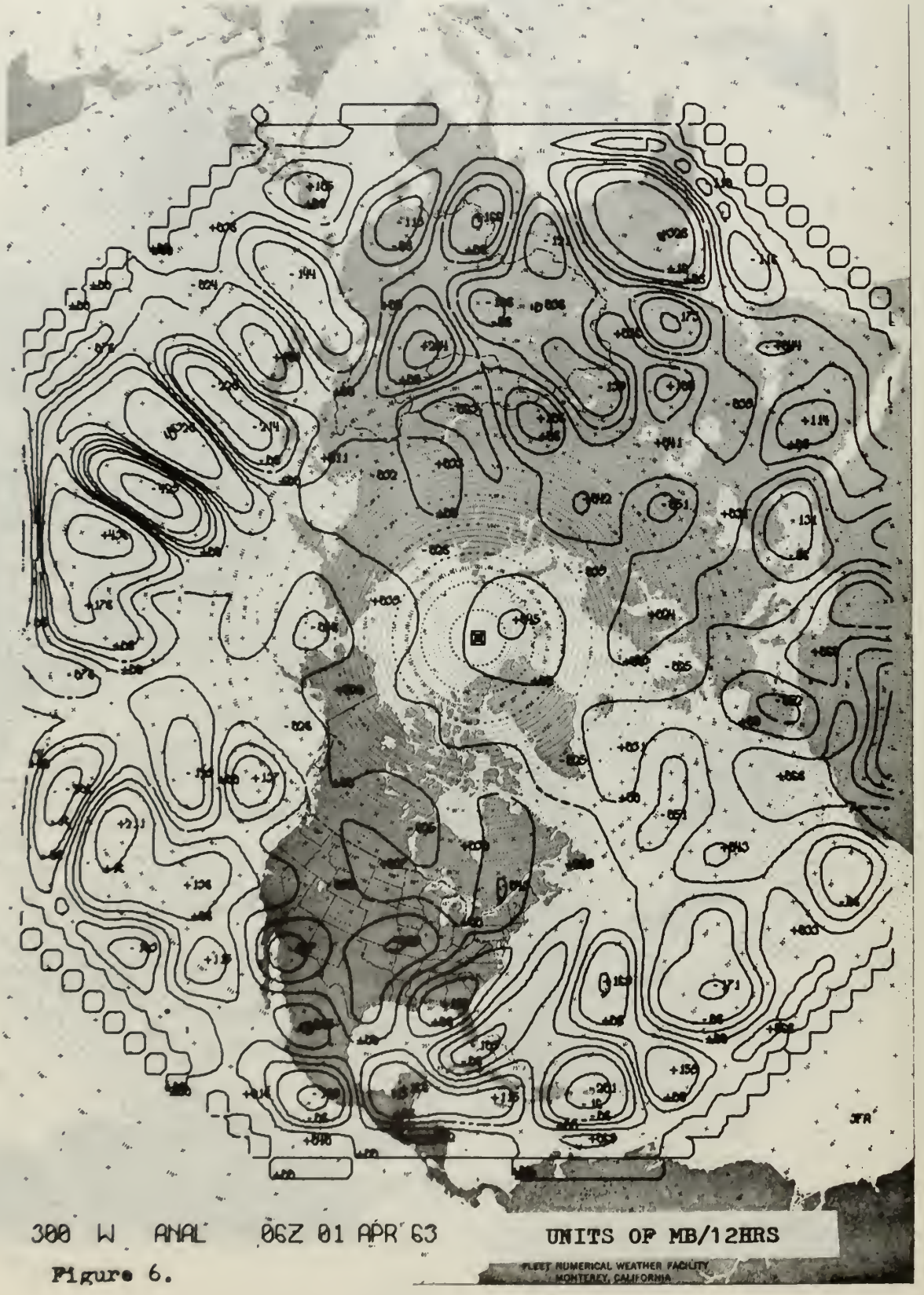
300 W ANAL 06Z 01 APR 63
UNITS OF MB/12HRS
FLEET NUMERICAL WEATHER FACILITY
MONTEREY, CALIFORNIA

Figure 6.


200 W ANAL 06Z 01 APR 63
UNITS OF MB/12HRS
FLEET NUMERICAL WEATHER FACILITY
MONTEREY, CALIFORNIA

Figure 7.


100 W ANAL 06Z 01 APR 63
UNITS OF MB/12HRS
FLEET NUMERICAL WEATHER FACILITY
MONTEREY, CALIFORNIA

Figure 8.


50 W ANAL 06Z 01 APR 63
UNITS OF MB/12HRS
FLEET NUMERICAL WEATHER FACILITY
MONTEREY, CALIFORNIA

Figure 9.

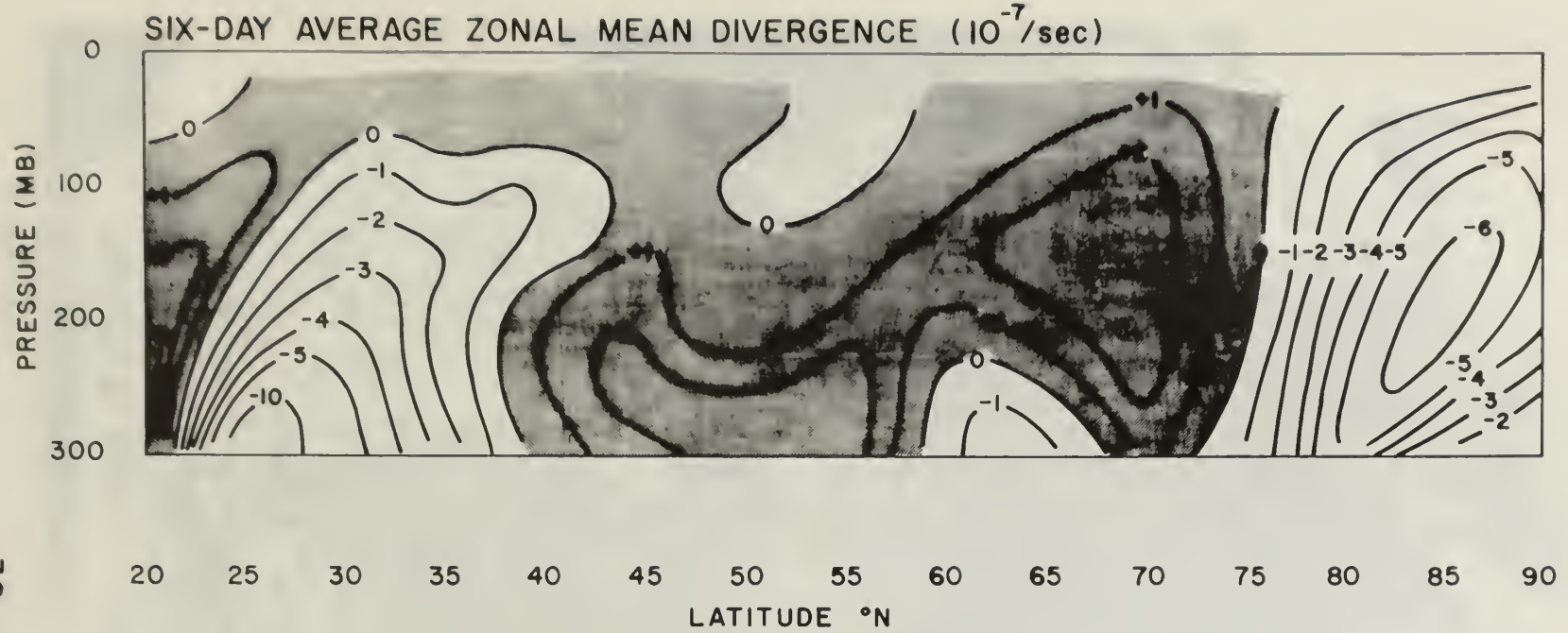

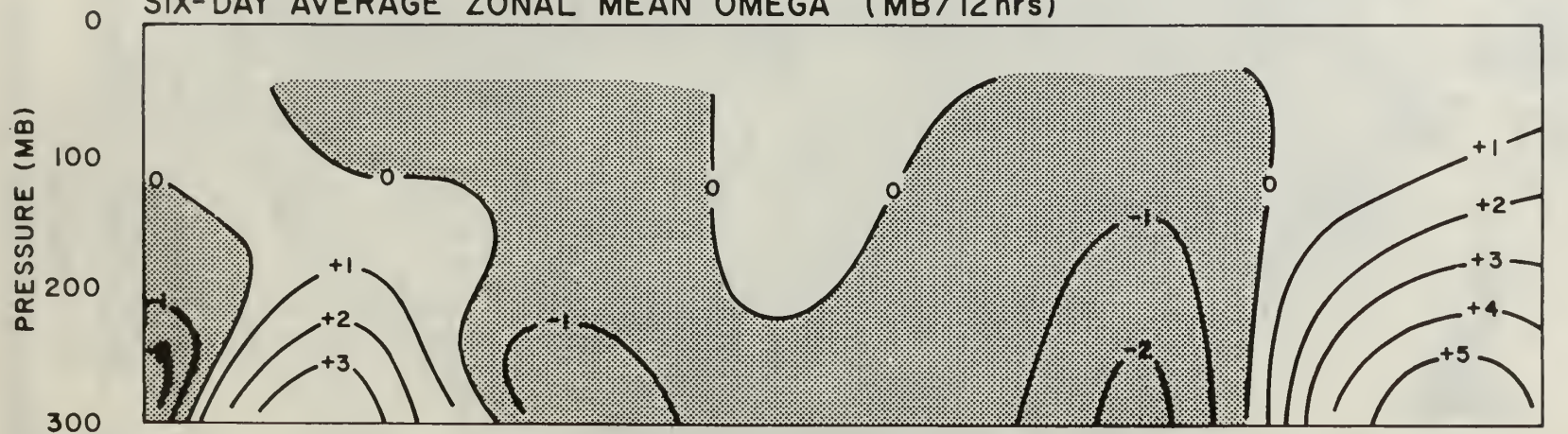

FIGURE 10 : MEAN NORTHERN HEMISPHERE MERIDIONAL PROFILES (1-6 APRIL 1963)

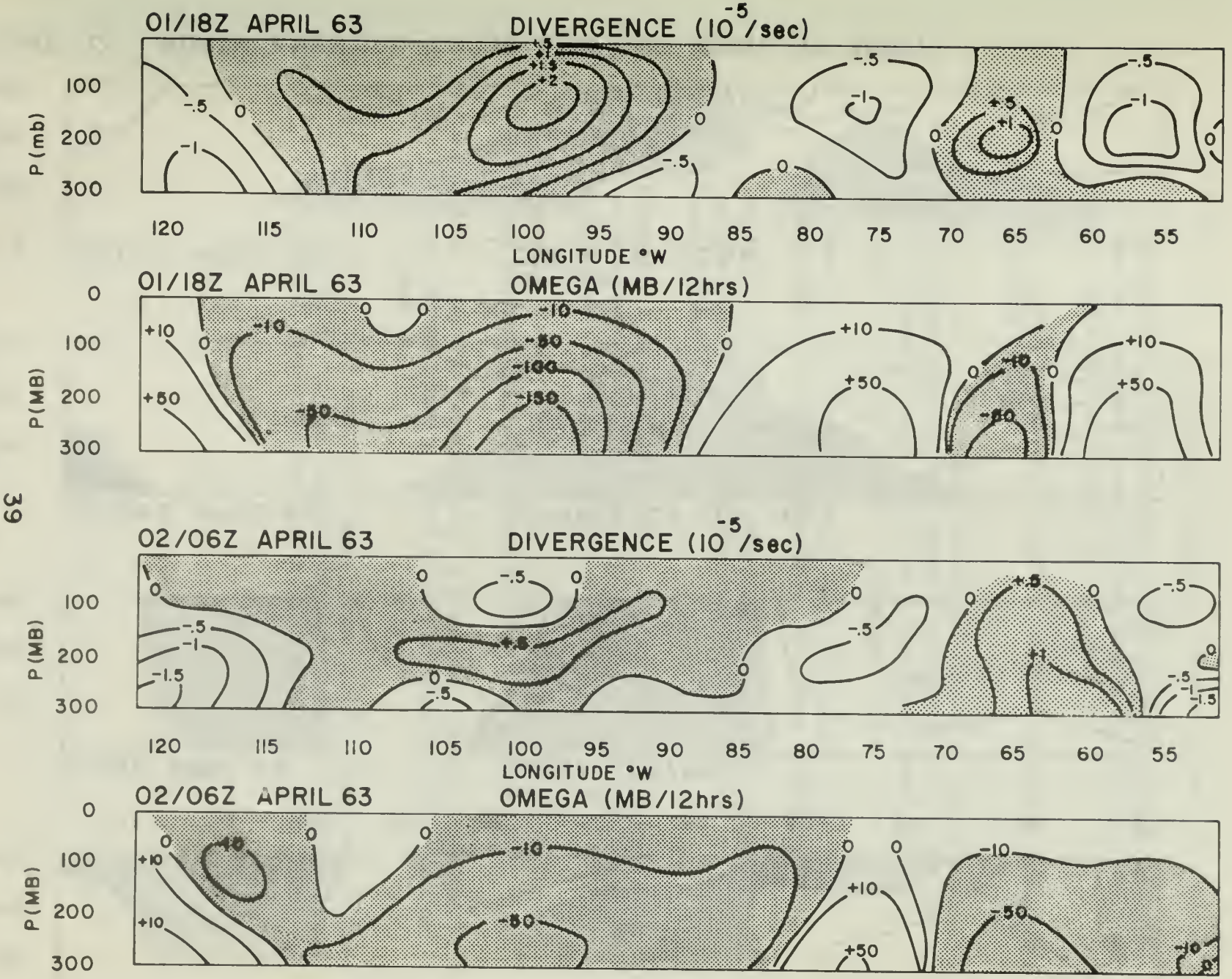

FIGURE 11. NORTH AMERICA CROSS SECTIONS WEST TO EAST

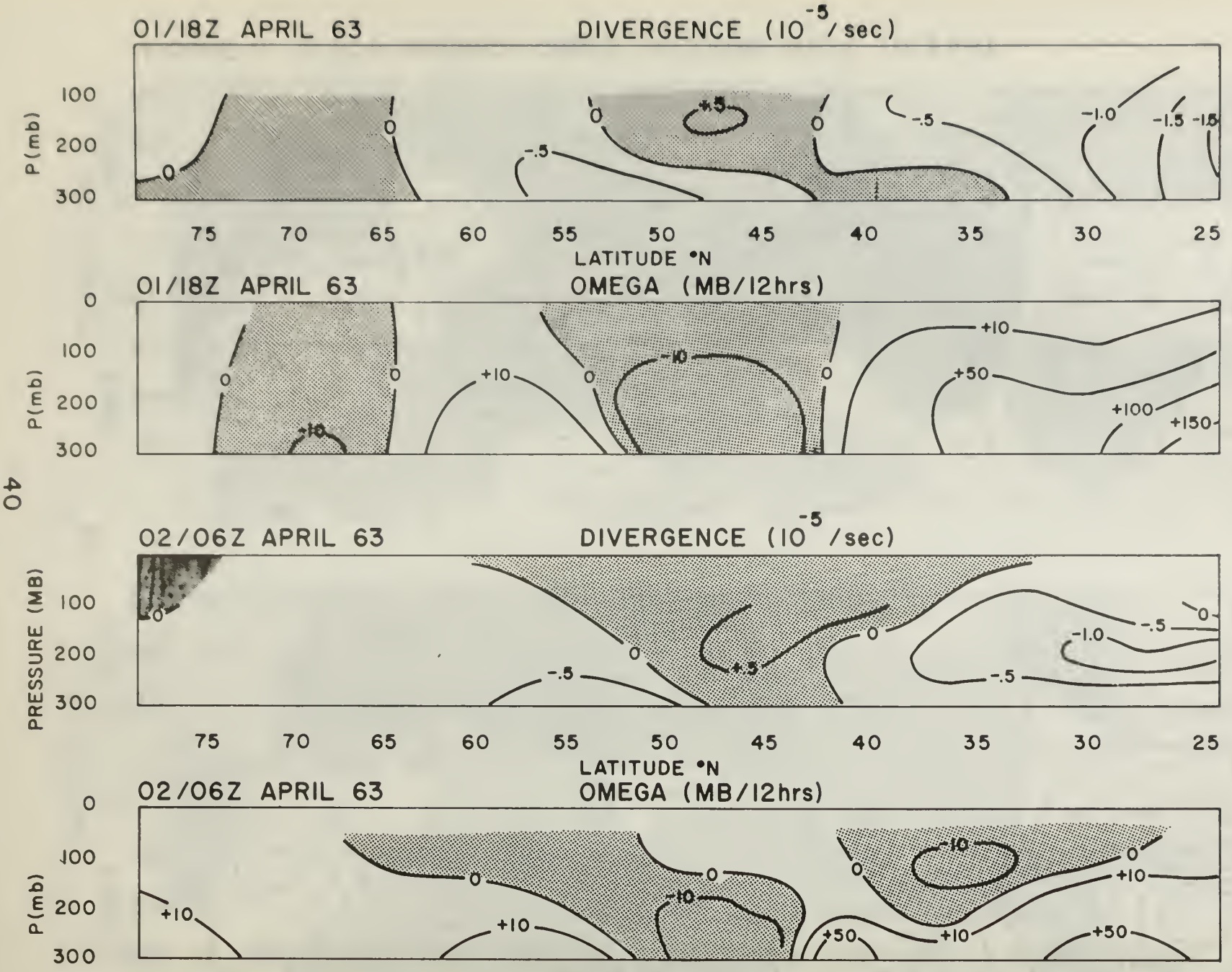

FIGURE 12. NORTH AMERICAN CROSS SECTIONS NORTH TO SOUTH

BIBLIOGRAPHY

1. Craig, R. A., The Upper Atmosphere. Academic Press Inc., 1965.

2. Cressman, G. P., A Three-Level Model Suitable for Daily Numerical Forecasting, National Meteorological Center, United States Weather Bureau Technical Memorandum No. 22, 1963.

3. Lorenz, E. N., Energy and Numerical Weather Prediction, Tellus 12, pp. 364-373, 1960.

4. Martin, F. L., A Diagnostic Method for Computing the 12-hour Mean Velocity Potential with Special Application to the layer 100-300 mb. Preprint memo. No. 64-6(b), National Center for Atmospheric Research, Boulder, Colorado, 1964.

5. Pantzke, E., Die Temperatur-und Windverhaltnisse in der Stratosphere uber Berlin im 1 Halbjar 1963, Band L/Heft 1,

6. Pressman, J., Seasonal and Latitudinal Temperature changes in the Ozonosphere. Journal of Meteorology, Vol. 12, No. 1, February 1955.

7. Scherhag, R., et. al., Tagliche Hokenkarten der 100-mbar-Flache sowie monatliche Mittelkarten, fur das Jahr 1963 Meteorologische Abhandlungen, Band XXVII/Heft 2, p. IV/1.

8. Scherhag, R., et. al., Tagliche und mittlere Boden-und 300-mb-Karten der Nordhemisphare, Band XXXV/Heft 4, p. IV/1, April, 1963.

9. Schuman, F. G., (unpublished): A Numerical solution-procedure for the Balance Equation. Joint Numerical Weather Prediction Unit, Washington, D. C.

10. Schuman, F. G., Numerical Experiments With the Primitive Equations. Proceedings of the International Weather Prediction in Tokyo, Nov. 7-13, 1960, Meteorological Society of Japan, Mar. 1962.

INITIAL DISTRIBUTION LIST

		No. Copies
1.	LCDR J. D. Jarrell, USN Navy Weather Research Facility Naval Air Station, Bldg. R-48 Norfolk, Virginia 23511	3
2.	F. L. Martin Environmental Sciences Naval Postgraduate School Monterey, California 93940	5
3.	Library Naval Postgraduate School Monterey, California 93940	2
4.	Department of Meteorology & Oceanography Naval Postgraduate School Monterey , California 93940	1
5.	Defense Documentation Center Cameron Station Alexandria, Virginia 22314	20
6.	Office of the Naval Weather Service Washington Navy Yard, blg. 200 Washington, D. C. 20390	1
7.	Chief of Naval Operations (Op-09B7) Navy Department Washington, D. C. 20350	1
8.	Officer in Charge Navy Weather Research Facility Naval Air Station, Bldg. R-48 Norfolk, Virginia 23511	1
9.	Commanding Officer and Director Navy Electronics Laboratory Attn: Code 2230 San Diego, California 92152	1
10.	Officer in Charge Fleet Numerical Weather Facility Naval Postgraduate School Monterey, California 93940	2

11.	Director, Naval Research Laboratory Attn: Tech Services Information Officer Washington, D. C. 20390	1
12.	Geophysics Research Directorate Air Force Cambridge Research Center Cambridge, Massachusetts	1
13.	Program Director for Meteorology National Science Foundation Washington, D. C.	1
14.	U. S. Department of Commerce Weather Bureau Washington, D. C.	2
15.	Office of Naval Research Department of the Navy Washington, D. C. 20360	1
16.	Naval Oceanographic Office Attn: Division of Oceanography Washington, D. C. 20390	1
17.	Office of Naval Research Attn: Geophysics Branch (Code 416) Department of the Navy Washington, D. C. 20360	1
18.	Program Director Oceanography National Science Foundation Washington, D. C.	1
19.	Director National Oceanographic Data Center Washington, D. C.	1
20.	Chairman Department of Meteorology & Oceanography New York University University Heights, Bronx New York, New York	1
21.	Director Scripps Institution of Oceanography University of California, San Diego La Jolla, California	1

22. Department of Meteorology & Oceanography — 1
Chairman
University of Hawaii
Honolulu, Hawaii

23. Department of Meteorology — 1
University of California
Los Angeles, California

24. Department of Geophysical Sciences — 1
University of Chicago
Chicago, Illinois

25. Department of Atmospheric Science — 1
Colorado State University
Fort Collins, Colorado

26. Department of Engineering Mechanics — 1
University of Michigan
Ann Arbor, Michigan

27. School of Physics — 1
University of Minnesota
Minneapolis, Minnesota

28. Department of Meteorology — 1
University of Utah
Salt Lake City, Utah

30. National Center for Atmospheric Research — 1
Boulder, Colorado

31. Department of Meteorology & Climatology — 1
University of Washington
Seattle, Washington 98105

32. Department of Meteorology — 1
University of Wisconsin
Madison, Wisconsin

33. Department of Meteorology — 1
Florida State University
Tallahassee, Florida

34. Department of Meteorology — 1
Massachussetts Institute of Technology
Cambridge, Massachussetts 02139

35. Department of Meteorology — 1
Pennsylvania State University
University Park, Pennsylvania

36. University of Oklahoma — 1
Research Institute
Norman, Oklahoma

37. Atmospheric Science Branch — 1
Science Research Institute
Oregon State College
Corvallis, Oregon

38. The University of Texas — 1
Electrical Engineering Research Laboratory
Engineering Science
Building 631A
University Station
Austin, Texas 78712

39. Department of Meteorology — 1
Texas A & M University
College Station, Texas 77843

40. Lamont Geological Observatory — 1
Columbia University
Palisades, New York

41. Division of Engineering and Applied Physics — 1
Room 206, Pierce Hall
Harvard University
Cambridge, Massachusetts

42. Department of Mechanics — 1
The Johns Hopkins University
Baltimore, Maryland

43. University of California — 1
E. O. Lawrence Radiation Laboratory
Livermore, California

44. Department of Astrophysics & Atmospheric Physics — 1
University of Colorado
Boulder, Colorado

45. Bureau of Meteorology — 1
Department of the Interior
Victoria and Drummond Streets
Carlton, Victoria, Australia

46. International Antartic Analysis Centre — 1
468 Lonsdale Street
Melbourne, Victoria, Australia

47. Department of Meteorology — 1
McGill University
Montreal, Canada

48. Central Analysis Office — 1
Meteorological Branch
Regional Adm. Building
International Airport
Dorval, Quebec, Canada

49. Meteorological Office — 1
315 Bloor Street West
Toronto 5, Ontario, Canada

50. Institut fur Theoretische Meteorologie — 1
Freie Universitat Berlin
Berlin-Dahlem
Thiel-allee 49
Federal Republic of Germany

51. Meteorological Service — 1
44, Upper O'Connell Street
Dublin 1, Ireland

52. Department of Meteorology — 1
The Hebrew University
Jerusalem, Isreal

53. Geophysical Institute — 1
Tokyo University
Bunkyo-ku
Tokyo, Japan

54. Department of Meteorology — 1
Instituto de Geofisica
Universidad Nacional de Mexico
Mexico 20, D.F., Mexico

55. New Zealand Meteorological Service — 1
P. O. Box 722
Wellington, G. E., New Zealand

56. Institute of Geophysics — 1
University of Bergen
Bergen, Norway

57. Department of Meteorology — 1
Imperial College of Science
South Kensington
London S. W. 7, United Kingdom

58. Meteorological Office — 1
London R
Bracknell
Berkshire, United Kingdom

59. Commonwealth Scientific and Industrial Research Organization — 1
314 Albert Street
East Melbourne, C. 2, Victoria

60. Director — 1
Pacific Oceanographic Group
Nanaimo, British Columbia
Canada

DOCUMENT CONTROL DATA - R&D

(Security classification of title, body of abstract and indexing annotation must be entered when the overall report is classified)

1. ORIGINATING ACTIVITY (Corporate author)
Naval Postgraduate School
Monterey, California 93940

2a. REPORT SECURITY CLASSIFICATION
Unclassified

2b. GROUP

3. REPORT TITLE
MODEL COMPUTATIONS OF VERTICAL MOTION IN THE UPPER TROPOSPHERE AND LOWER STRATOSPHERE FROM WIND POTENTIAL DATA

4. DESCRIPTIVE NOTES (Type of report and inclusive dates)
Thesis

5. AUTHOR(S) (Last name, first name, initial)
JARRELL, Jerry Dean, Lieutenant Commander, United States Navy

6. REPORT DATE	7a. TOTAL NO. OF PAGES	7b. NO. OF REFS
June 1967	46	10

8a. CONTRACT OR GRANT NO.

b. PROJECT NO.

c.

d.

9a. ORIGINATOR'S REPORT NUMBER(S)

9b. OTHER REPORT NO(S) (Any other numbers that may be assigned this report)

10. AVAILABILITY/LIMITATION NOTICES
[redacted]

11. SUPPLEMENTARY NOTES

12. SPONSORING MILITARY ACTIVITY

13. ABSTRACT

Fields of the potential function which had been obtained previously by Martin (1964), by numerical solution of a Poisson type equation were employed in this paper to obtain the divergence of the wind field at each grid point. Based upon a vertical interpolating polynomial formula for divergence, vertical integration of the divergence fields is performed from the top of the atmosphere to determine values of vertical motion at each grid point on the 50, 100, 200, and 300 mb levels. Features of these fields are discussed.

14 KEY WORDS	LINK A		LINK B		LINK C	
	ROLE	WT	ROLE	WT	ROLE	WT
DIAGNOSTIC VERTICAL MOTIONS						
VELOCITY POTENTIAL FUNCTION						
INTEGRATED CONTINUITY EQUATION						
VERTICALLY INTEGRATED DIVERGENCE						
STRATOSPHERIC OMEGA FIELDS						